Title: Graphitic carbon nitride co-modified by zinc phthalocyanine and graphene quantum dots for the efficient photocatalytic degradation of refractory contaminants

Authors: Tiefeng Xu, Dongni Wang, Lulu Dong, Haibin Shen, Wangyang Lu, Wenxing Chen

PII: S0926-3373(18)31099-3
DOI: https://doi.org/10.1016/j.apcatb.2018.11.049
Reference: APCATB 17215

To appear in: *Applied Catalysis B: Environmental*

Received date: 20 August 2018
Revised date: 23 October 2018
Accepted date: 16 November 2018

Please cite this article as: Xu T, Wang D, Dong L, Shen H, Lu W, Chen W, Graphitic carbon nitride co-modified by zinc phthalocyanine and graphene quantum dots for the efficient photocatalytic degradation of refractory contaminants, *Applied Catalysis B: Environmental* (2018), https://doi.org/10.1016/j.apcatb.2018.11.049

Graphitic carbon nitride co-modified by zinc phthalocyanine and graphene quantum dots for the efficient photocatalytic degradation of refractory contaminants

Tiefeng Xu, Dongni Wang, Lulu Dong, Haibin Shen, Wangyang Lu,† Wenxing Chen

†

National Engineering Lab for Textile Fiber Materials & Processing Technology (Zhejiang),

Zhejiang Sci-Tech University, Hangzhou 310018, China

Graphical Abstract

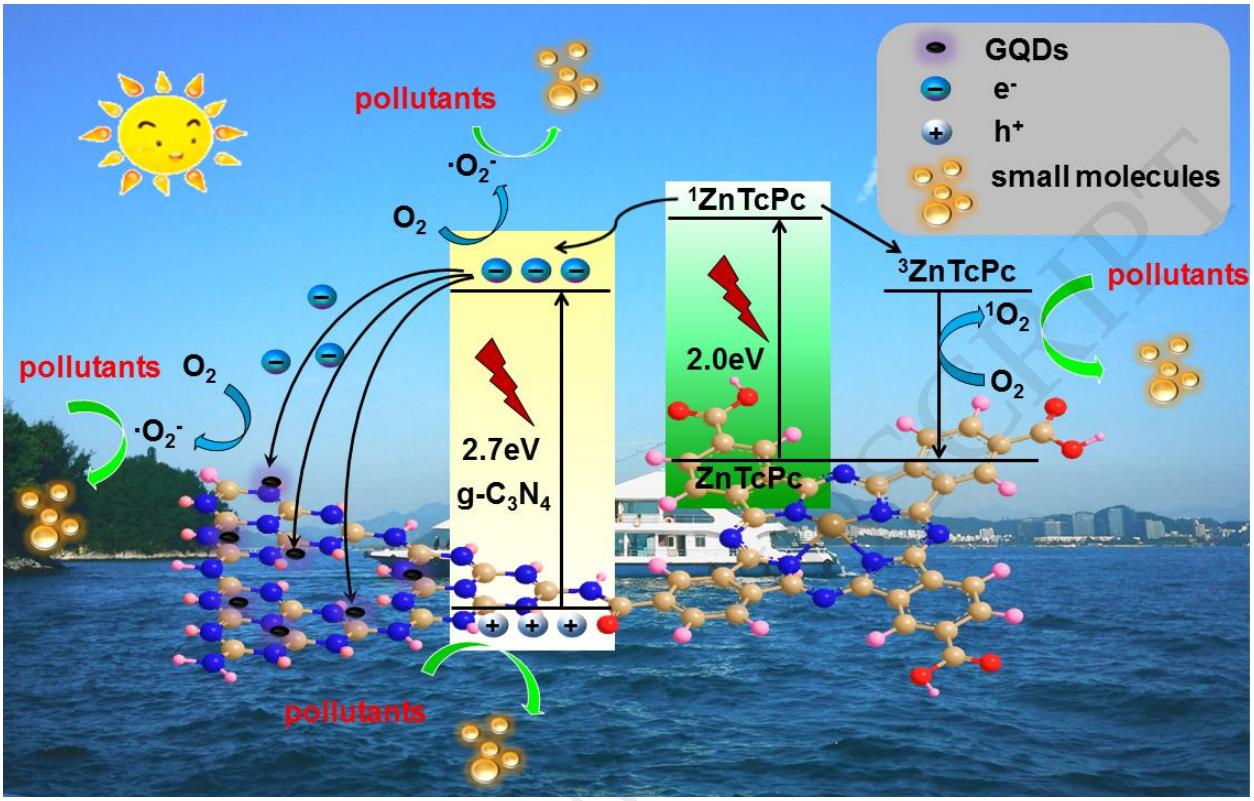

Highlights

- g-C_3N_4 co-modified by zinc phthalocyanine and graphene quantum dots was prepared.
- The enhanced photocatalytic activity of refractory contaminants.
- The increased visible-light response and effective charge separation were achieved.
- The degradation pathways of RhB and SQXNa were proposed.

Abstract

Broad solar light absorption and rapid photogenerated electron-hole pair separation are two critical factors for the efficient enhancement of catalytic performance in a g-C_3N_4-based photocatalytic system. This study developed a facile method to construct a ternary graphitic carbon nitride/zinc tetracarboxyphthalocyanine/graphene quantum dots (g-C_3N_4/ZnTcPc/GQDs) composite photocatalyst. Graphene quantum dots (GQDs) were used to modify g-C_3N_4/ZnTcPc through hydrothermal method, where g-C_3N_4/ZnTcPc was fabricated by immobilizing zinc tetracarboxyphthalocyanine (ZnTcPc) onto g-C_3N_4 covalently via amido bonds. The photocatalyst was characterized by transmission electron microscopy, ultraviolet-visible diffuse reflectance spectrum, and X-ray photoelectron spectroscopy. The g-C_3N_4/ZnTcPc/0.1GQDs composites presented an increased photocatalytic activity by using Rhodamine B, sulfaquinoxaline sodium and carbamazepine as the model pollutants under solar light irradiation. ZnTcPc bonding on the g-C_3N_4 broadens its visible-light spectral response, and GQDs promotes the photogenerated electron-hole-pair separation efficiency because of its efficient electrons-transfer property. Experiments confirmed that superoxide radicals, photogenerated holes and singlet oxygen are the primary active species. The photocatalytic degradation pathway of both Rhodamine B, sulfaquinoxaline sodium and carbamazepine was proposed on the basis of ultra-performance liquid chromatography and high-definition mass spectrometry.

Keywords: graphitic carbon nitride, phthalocyanine, graphene quantum dots, electron transfer, degradation pathway

1. Introduction

Abundant poisonous and refractory pollutants such as pharmaceuticals and personal care products [1], and some organic conjugate compounds in the environment are produced accompanied by rapid industrial development and population growth. These pollutants have become a severe global environmental problem [2, 3]. An awareness of the presence of these hazardous pollutants in the environment, including in surface water, groundwater, and particularly in wastewater should initiate precautionary management action to reduce disastrous impacts on the environment [4-6]. Semiconductor photocatalysis can be considered an ideal and feasible strategy for environmental governance, particularly to remove poisonous and refractory organic compounds from wastewater [7-9].

Graphitic carbon nitride (g-C_3N_4) [10] as a metal-free organic-polymeric semiconductor with a visible-light response, has attracted widespread concern in photocatalytic hydrogen generation [11-13], CO_2 photocatalytic conversion [14-16] and organic contaminant degradation [17, 18], because of its merits of environmental friendliness, reliable stability and adjustable electronic properties. Meanwhile, g-C_3N_4 as two-dimensional material can provide enough reactive sites on

the surface. Nevertheless, two primary characteristics restrict its photocatalytic activity, namely, a comparatively unsatisfactory utilization of solar light and the rapid recombination of photogenarated electron-holes pair. Various strategies have been exploited to overcome these issues, and improvements in g-C_3N_4 have resulted, including its coupling with other semiconductors [19-21], doping with non-metallic or metallic elements [22-25], fabrication of different morphologies [26-29] and sensitization with compounds [30-32]. Metal phthalocyanine (MPc) is a well-known chromophore and it can be exploited as a dye for the sensitization of semiconductors that are absorbed internally in the visible region with the Soret band in the ultraviolet/blue spectral regions and the Q band centered at ~650-800 nm in the red/near infrared (NIR) spectral regions [33-35]. MPc are favorable catalysts because of their accessibility and excellent photochemical and thermal stabilities [36]. In our previous study, the breakthrough of ZnPc as sensitizer was achieved in g-C_3N_4-based photocatalytic systems to eliminate poisonous organic pollutants [37]. The sensitization of ZnPc can widen the visible-light response range of g-C_3N_4 from 450 nm to more than 700 nm.

However, it is a biggest obstacle to achieve the extension of visible light response and the effective charge separation simultaneously in the binary photocatalytic system. The effective separation of photogenerated carriers must be implemented to increase the photocatalytic activity, where photogenerated electron-hole pair should be separated and transferred into the valence band (VB) and conduction band (CB) of opposite semiconductor. Carbon materials are

appropriate candidates because of their superior optical and excellent electron-transfer properties, including carbon nanotube [38, 39], carbon quantum dots [40, 41], graphene [42], and graphene quantum dots [43, 44]. Among them, graphene quantum dots (GQDs) with dimensions less than 10 nm in diameter possess a unique character and have attracted attention to improve the photocatalytic performance of semiconductor materials. It is promising that g-C_3N_4-based binary photocatalysts can be combined with highly conductive GQDs by electrostatic, π-π stacking and hydrogen-bonding interactions. Because of its nanoscale, it can be distributed evenly on the g-C_3N_4 surface without affecting the photocatalyst ability to absorb light.

Herein, we prepared a ternary g-C_3N_4/zinc phthalocyanine/graphene quantum dots (g-C_3N_4/ZnTcPc/GQDs) composite photocatalyst by dye sensitization and modification with carbon materials, and applied this catalyst to degrade Rhodamine B (RhB), sulfaquinoxaline sodium (SQXNa) and carbamazepine (CBZ) under solar light irradiation. The morphology structures, chemical components, and optical properties of the composite photocatalyst were investigated via a series of characterizations, and the effects of the amounts of GQDs, pH, and catalyst stability are discussed. An increased visible-light spectral response and effective charge separation are achieved simultaneously in the ternary photocatalytic system. Additionally, the existence of superoxide radicals ($\bullet O_2^-$), photogenerated holes (h^+) and singlet oxygen ($^1O_2$) has been evidenced in the g-C_3N_4/ZnTcPc/GQDs catalytic system. A feasible photocatalytic mechanism of g-C_3N_4/ZnTcPc/GQDs has been proposed. The photocatalytic degradation

pathway for RhB, SQXNa and CBZ was proposed based on the detection of intermediates through ultra-performance liquid chromatography and high-definition mass spectrometry (UPLC/HDMS).

2. Experimental

2.1 Photocatalyst preparation

g-C_3N_4 and ZnTcPc were synthesized according to the literature with modifications [45-47]. g-C_3N_4 was prepared by a facile calcination strategy of urea. The urea in a covered crucible was heated at 550°C for 3 h at 2.5°C/min in a tube furnace. After being cooled to room temperature, the resulting faint yellow powder was collected for further use. The synthetic method and optimal ratio of g-C_3N_4/ZnTcPc composite photocatalysts were consistent with previous literature methods [37].

g-C_3N_4/ZnTcPc/GQDs composite photocatalysts were fabricated via a hydrothermal method. First, the as-prepared g-C_3N_4/ZnTcPc (200 mg) and a certain amount of GQDs aqueous solution (0.12 mL, 0.16 mL, 0.20 mL, 0.24 mL, 0.28 mL, 1 mg/mL) were dispersed in a mixture solution of ethanol and water with ultrasonication for 1h in a typical synthesis, where the volume ratio of water and alcohol was 4:3. The disperse solution was treated at 453 K for 3 h in a Teflon-lined stainless steel autoclave. The final product was collected by centrifugation, washed three times with ultrapure water and ethanol, and then dried by freeze drying at 223 K for 18 h. The obtained

samples were termed g-C_3N_4/ZnTcPc/0.06GQDs, g-C_3N_4/ZnTcPc/0.08GQDs, g-C_3N_4/ZnTcPc/0.1GQDs, g-C_3N_4/ZnTcPc/0.12GQDs and g-C_3N_4/ZnTcPc/0.14GQDs for the GQDs feeding amount of 0.12 mL, 0.16 mL, 0.20 mL, 0.24 mL, 0.28 mL, respectively. The preparation process of the g-C_3N_4/ZnTcPc/GQDs composite photocatalysts is depicted in **Scheme 1**.

2.2 Characterization

Transmission electron microscope (TEM) and high resolution transmission electron microscopy (HRTEM) graph (JEOL, JEM-2010) were obtained to study the morphology and microstructure images. Ultraviolet-visible diffuse reflection spectra (UV-vis DRS) were obtained from 300–800 nm with a Hitachi UH4150 spectrometer. Fourier-transform infrared spectroscopy (FTIR) spectra were recorded using a Thermo Nicolet 5700 analyzer to investigate the structure of as-prepared samples. The chemical environments of the as-prepared photocatalysts were analyzed by X-ray photoelectron spectroscopy (XPS) (Thermo Fisher Scientific) with a monochromatic Al-Kα source operated at 1486.6 eV. The crystal structures of the photocatalysts were performed by X-ray diffraction (XRD) using a Bruker AXS D8-discover diffractometer operating with Cu-Kα radiationin in the range of 2θ from 5° to 50°. The total organic carbon (TOC) content of the samples was analyzed by a liquiToc-2 analyzer (Elementar, Germany).

The photoelectrical properties were measured on a CHI660E electrochemical workstation (Chenhua Instrument) using 0.1 M Na_2SO_4 as an electrolyte solution including a three-electrode

cell system with the prepared photocatalysts on carbon paper as the working electrode, an Ag/AgCl wire (saturated KCl solution) as reference electrode, and Pt wire as the counter electrode. The light source was a 100 W lamp (LOT-oriel GmbH & Co. KG). The working electrodes were prepared as follows: catalyst was dispersed into a mixed solution of ultrapure water, isopropanol and perfluorosulfonic acid polymer (Nafion), then the suspension was spread onto a 1 cm × 5 cm carbon paper substrate and dried at 60°C. Electron paramagnetic resonance (EPR) technology (Bruker A-300) was used to confirm the possible active species under solar light irradiation. The settings for the EPR spectrometer were as follows: sweep width, 100 G; microwave frequency, 9.86 G; modulation frequency, 100 kHz; power, 20 mW.

2.3 Photocatalytic experiments

Photocatalytic measurements of the as-prepared catalysts were conducted by using different organic pollutants as the target pollutants with a Q-Sun Xe-1 test chamber (USA), with RhB was an organic conjugate compound, and SQXNa and CBZ were the representative antibiotic and antiepileptic drugs respectively. The spectral power distribution of the Q-SUN Xe-1 is shown in **Fig. S1**. Substrate aqueous solution (20 mL, 2×10^{-5} mol/L) that contains 2 mg of photocatalyst (0.1 g/L) was transferred into the reactor. Prior to light irradiation, the mixture was treated by ultrasonication for 10 min in the dark to obtain a uniform suspension. At a certain time interval, the solution was removed continually from the reactor and filtered to remove the photocatalyst particles. The RhB concentration was determined by UV-vis spectrometry (Hitachi, U3900H) at

554 nm, and the concentrations of CBZ and SQXNa were monitored by ultra-performance liquid chromatography with a PDA detector (UPLC, Waters). The reaction system pH was adjusted by H_2SO_4 or NaOH addition.

2.4 Analytical methods

The degradation intermediates and final products of RhB, SQXNa and CBZ over g-C_3N_4/ZnTcPc/GQDs were analyzed by UPLC/HDMS (Waters, Synapt G2-S) with an electrospray ionization (ESI) source. A HSS T3 column (1.8 μm, 2.1×100 mm) was used to separate the relevant components at a flow rate of 0.4 mL/min. In positive mode, the mobile phase was composed of water (solvent A) and acetonitrile or methanol (RhB: methanol, SQXNa and CBZ: acetonitrile, solvent B). An eluent gradient schedule for the intermediates detection of RhB was used during the separation: from 0 to 1.0 min, 60% A; from 1.0 to 7.0 min, 60%-30% A (linear); from 7.0 to 8.0 min, 30% A; from 8.0 to 8.1 min, 30%-60% A (linear); and from 8.1 to 10.0 min, 60% A. The eluent gradient schedule for the intermediates detection of SQXNa and CBZ was as follows: from 0 to 0.3 min, 90% A; from 0.3 to 8 min, 90%-10% A (linear); from 8.0 to 9.0 min, 10% A; from 9.0 to 9.1 min, 10%-90% A(linear); and from 9.1 to 10.0 min, 90% A. In negative mode, the mobile phase was composed of water or acidified water (0.1% formic acid, solvent A) and methanol (solvent B). An eluent gradient schedule was used during the separation: from 0 to 0.2 min, 99% A; from 0.2 to 6 min, 99%-80% A (linear); from 6 to 8.5 min, 80%-40% A (linear); from 8.5 to 9.0 min, 40% A; from 9.0 to 9.1 min, 40%-99% A(linear); and

from 9.1 to 10 min, 99% A. The source and desolvation temperature were set to 120°C and 500°C, respectively. Nitrogen was used as the cone gas (50.0 L/h) and desolvation gas (600.0 L/h). The scan range was set to m/z 50–1200.

3. Results and discussion

3.1 Characterization

The morphology and microstructure of as-prepared g-C_3N_4, g-C_3N_4/ZnTcPc and g-C_3N_4/ZnTcPc/GQDs were exhibited by TEM in **Fig. 1a-i**. According to the TEM images (**Fig. 1a-c.**), g-C_3N_4 has a thin lamellar structure, which could lead to a larger specific surface area and more reactive sites. When ZnTcPc was immobilized onto g-C_3N_4 covalently via amido bonds, **Fig.1d-f** shows that the lamellar structure of g-C_3N_4 has no apparent difference before and after the introduction of ZnTcPc. No ZnTcPc is visible in the TEM or HMTEM images (**Fig.1f**), which indicated that ZnTcPc did not exist in crystals but exists as small molecules. **Figure 1h** shows that the GQDs were well dispersed uniformly and the g-C_3N_4 was covered by numerous GQDs. In accordance with previous work, the relatively low contrast degree of the TEM image was assigned to the single-layered or few-layered structure of the GQDs [48]. **Figure 1i** shows that the GQDs were well anchored on the g-C_3N_4 nanosheet surface and the average GQD size was ~2-6 nm.

The DRS spectra of as-prepared samples in **Fig. 2** were used to study their optical properties, and they showed the effect of ZnTcPc and GQDs on the visible-light absorption range of g-C_3N_4. The pure g-C_3N_4 possessed an absorption edge at ~460 nm, which corresponded to its relatively large bandgap energy of 2.7 eV. g-C_3N_4/ZnTcPc revealed a better visible light absorption, where the maximum absorption wavelength was ~700 nm. The g-C_3N_4/ZnTcPc/GQDs photocatalyst also maintained superior visible-light-absorption properties. Therefore, we concluded that ZnTcPc broadened the visible-light response range of g-C_3N_4 and the strong electron-transfer interaction between g-C_3N_4/ZnTcPc and GQDs may induce a synergetic effect to enhance the photoactivity of g-C_3N_4/ZnTcPc.

Additionally, the structure of as-prepared catalysts was analyzed by FT-IR (**Fig. 3a**). In the FT-IR spectrum of ZnTcPc, the intensive band at ~1705 cm^{-1} was indicative of the absorption by carbonyl stretching. The characteristic peaks at ~1087, 1250, 1345 and 1522 cm^{-1} may be related to the skeleton stretching of ZnTcPc [49, 50]. Pure g-C_3N_4 exhibited characteristic FT-IR absorption peaks similar to that in previous reports [51, 52]. The characteristic peak at 814 cm^{-1} corresponded to typical tri-s-striazine ring units. The absorption peaks for pure g-C_3N_4 in the region of 1200-1600 cm^{-1} were ascribed to the classical stretching modes of C-N heterocycles. Peaks from 3000 and 3600 cm^{-1} were caused by the existence of stretching modes of terminal NH_2 or NH groups that originated from the defect sites of the aromatic ring. The characteristic peaks of g-C_3N_4/ZnTcPc and g-C_3N_4/ZnTcPc/0.1GQDs were similar to those of g-C_3N_4.

However, the characteristic peaks of ZnTcPc and GQDs could not be detected from the FTIR spectra of g-C_3N_4/ZnTcPc and g-C_3N_4/ZnTcPc/0.1GQDs, because of their trace amount and the strong stretching vibration peaks of g-C_3N_4.

The phase and structure of ZnTcPc, g-C_3N_4, g-C_3N_4/ZnTcPc and g-C_3N_4/ZnTcPc/0.1GQDs were measured by XRD. As shown in **Fig. 3b**, two distinct diffraction peaks at 13.1° and 27.5° for g-C_3N_4 agreed well with the reported standard, which corresponded to the (100) and (002) planes of g-C_3N_4 (JCPDS 87-1526) [44]. It is assigned to the characteristic graphitic-like layered stacking of CN-based materials. The g-C_3N_4/ZnTcPc and g-C_3N_4/ZnTcPc/0.1GQDs composites showed no obvious characteristic peaks attributed to ZnTcPc and GQDs, which may occur due to the low loading content and low crystallinity of ZnTcPc and GQDs in the as-prepared g-C_3N_4/ZnTcPc/0.1GQDs composite. This is consistent with the observation from FT-IR. Meanwhile, the ZnTcPc and GQDs modification has no significant influence on the graphitic-like layered stacking structure of g-C_3N_4.

The surface chemical composition of the as-prepared catalysts, and the chemical interactions between g-C_3N_4/ZnTcPc and GQDs were explored by XPS analysis. **Figuer 4** and **S2** present the C1s and N1s XPS spectra of g-C_3N_4, g-C_3N_4/ZnTcPc and g-C_3N_4/ZnTcPc/0.1GQDs. As shown in **Fig. 4a**, the C 1s spectra of pure g-C_3N_4 could be split into three species at 284.6, 286.0, and 288.2 eV, which were attributed to C–C, C–NH_2 and N–C=N, respectively [53]. The C–NH_2 peak of g-C_3N_4/ZnTcPc/0.1GQDs was shifted to 285.7 eV, and the C–C peak of

g-C_3N_4/ZnTcPc/0.1GQDs was elevated in comparison with the N–C=N peak (**Fig. 4c**). This may be due to the addition of GQDs, which possess many C-COOH and C-C bonds, and showed the co-existence of GQDs and g-C_3N_4/ZnTcPc in the composites, which indicated a good agreement between the observed TEM results. Specifically, the N 1s peaks of all prepared catalysts may be deconvoluted to four species peaks at 398.7, 399.9, 401.0 and 404.2 eV. The signal peak at 398.7 eV corresponds to sp^2-hybridized nitrogen atoms in the triazine ring (C=N-C), which was consistent with the observation from the FT-IR analysis. The peak at 399.9 eV was attributed to the tertiary nitrogen bond to carbon atoms in N-$(C)_3$ or H-N-$(C)_2$, and the peak at 401.0 eV represented the amino function that carried hydrogen (C–N–H) of pure g-C_3N_4 in the aromatic cycles and the nitrogen of the amide group (–NH–CO–) formed for the bonding between the -NH_2 and -COOH [37]. The weaker peak at 404.4 eV may be assigned to π-excitation. Taken together, these conclusions obtained in studies confirmed g-C_3N_4/ZnTcPc/GQDs has been synthesized successfully and it has the potential enhanced photocatalytic performance.

3.2 Photocatalytic activity

RhB, colorless SQXNa and CBZ were used to evaluate the photocatalytic activity of the as-prepared catalysts under solar light irradiation. Above all, **Figure S3** depicts the photocatalytic performance of g-C_3N_4/ZnTcPc/GQDs catalysts with different quantities of GQDs for RhB degradation. The photocatalytic efficiency of RhB increased gradually with larger quantities of GQDs, from 0.06 wt% to 0.1 wt%. However, a further GQDs loading increase

resulted in a constant or further decreased degradation activity, which might be attributable to competition for light absorption between GQDs and g-C_3N_4, which reduced the formation of reactive species. Consequently, a suitable ratio between g-C_3N_4/ZnTcPc and GQDs is conducive to improve the photocatalytic activity and g-C_3N_4/ZnTcPc/0.1GQDs was chosen for further study. In **Fig. 5a**, the removal rate of RhB degradation almost had no change without any photocatalyst, which indicated that the direct photolysis of RhB could not be happened under solar light irradiation. ZnTcPc could barely degrade RhB, and g-C_3N_4 revealed an RhB removal rate of 44.7% within 60 min, whereas g-C_3N_4/ZnTcPc presented a removal efficiency of 73.1% for RhB degradation under the same conditions in **Fig. 5a**. Besides, g-C_3N_4/ZnTcPc/0.1GQDs exhibited no catalytic activity in the absence of a light source, which demonstated that the catalysts had no adsorption toward the target substrate and the catalytic oxidation reaction must be driven by a light source. When g-C_3N_4/ZnTcPc/0.1GQDs was present, the removal rate of RhB exceeded 98.2%, which was approximately 2 times the photonic efficiency than that of pure g-C_3N_4. This result implied that g-C_3N_4/ZnTcPc/0.1GQDs possessed a higher catalytic oxidation capacity. In addition, the photocatalytic performance of g-C_3N_4/ZnTcPc/0.1GQDs was superior to a physical mixture of g-C_3N_4/ZnTcPc and the same amount of GQDs (g-C_3N_4/ZnTcPc+0.1GQDs), which revealed a synergetic catalytic effect in the g-C_3N_4/ZnTcPc/0.1GQDs system. Besides, g-C_3N_4/ZnTcPc/0.1GQDs also exhibited a better photocatalytic activity of SQXNa within 40 min and CBZ within 180 min (**Fig. 5b**), which eliminated the sensitization effect on the degradation of RhB. The visible-light photocatalytic

performances (λ > 420 nm) of g-C_3N_4/ZnTcPc/0.1GQDs towards the degradation of RhB, SQXNa, and CBZ are shown in **Fig. S4.** g-C_3N_4/ZnTcPc/0.1GQDs also possesses photocatalytic activity under visible light irradiation (λ > 420 nm). From the above results, we inferred that the synergistic effect between g-C_3N_4 with ZnTcPc and GQDs resulted in the enhanced activities of g-C_3N_4/ZnTcPc/GQDs, which will be confirmed in the following experiments. The degree of mineralization is important for evaluating the complete degradation of organic pollutants. Therefore, the TOC removal ratios of RhB, CBZ and SQXNa over g-C_3N_4/ZnTcPc/0.1GQDs are shown in **Fig. S5**. About 48% of RhB, and 63% SQXNa are mineralized to CO_2 and H_2O under solar light irradiation for 60 min and 40 min, respectively. And about 59% of CBZ are removed under solar light irradiation for 180 min. The mineralization process indicates that the g-C_3N_4/ZnTcPc/0.1GQDs photocatalyst has mineralization ability.

Because the reaction kinetics of catalytic oxidation is often affected by pH, the photocatalytic degradation of RhB in the g-C_3N_4/ZnTcPc/0.1GQDs system was explored at various pH values. The RhB removal rates remained relatively high over a wide pH range. In contrast, g-C_3N_4/ZnTcPc/0.1GQDs showed a better activity for the photocatalytic degradation of RhB in acidic and neutral conditions, than in alkaline condition as shown in **Fig. 5c**. Moreover, the catalyst stability is critical to assess its practical application, and thus, recycling experiments of g-C_3N_4/ZnTcPc/0.1GQDs were performed over nine reaction runs under uniform conditions. As shown in **Fig. 5d**, it could be observed that it displays no obvious deactivation after nine

consecutive recycles for RhB degradation under solar light irradiation (each run lasted for 60 min), which disclosed that g-C_3N_4/ZnTcPc/0.1GQDs possessed an excellent chemical stability and reliability for practical application. The XRD and FT-IR of the fresh and used g-C_3N_4/ZnTcPc/0.1GQDs catalysts (before and after the ninth run cycle) were provided to highlight its stability (**Fig. S6**). It can be found that the structure and crystal phase had almost no apparent discrepancy between the fresh and used g-C_3N_4/ZnTcPc/0.1GQDs composite. XPS was further employed to confirm the chemical composition of the used g-C_3N_4/ZnTcPc/0.1GQDs after RhB degradation. The C1s peaks in the XPS spectrum (**Fig. S7**) presented a similar result to the fresh g-C_3N_4/ZnTcPc/0.1GQDs. The results pointed out that the catalyst is stable even after the ninth cycle of photocatalytic degradation.

3.3 Mechanism and pathway

3.3.1 Mechanism

EPR spin-trap technique tests were carried out in the photoreaction of g-C_3N_4/ZnTcPc/0.1GQD to achieve a better understanding of the possible reactive radicals. As a spin-trapping reagent, DMPO was exploited to capture •OH and •O_2^- [54, 55]. As depicted in **Fig. 6a**, the water-dispersion liquid of the g-C_3N_4/ZnTcPc and g-C_3N_4/ZnTcPc/0.1GQDs composites was irradiated for 2 min and no •OH signals were detected, whereas •OH was generated in the g-C_3N_4 photocatalytic system. Hence, we concluded that •OH was not a species in the g-C_3N_4/ZnTcPc/0.1GQDs photocatalytic reaction system. Four characteristic peaks of

DMPO-•O_2^- were observed in the g-C_3N_4/ZnTcPc/0.1GQDs system under solar light irradiation in **Fig. 6b**. •O_2^- was generated via a single-electron reduction process. •O_2^- produced during the g-C_3N_4 photocatalytic process was weaker than that of the g-C_3N_4/ZnTcPc and g-C_3N_4/ZnTcPc/0.1GQDs system, and its production could be ascribed to the electron transfer between g-C_3N_4 with ZnTcPc and GQDs. The participation of $^1O_2$ was also confirmed using 2,2,6,6-tetramethylpiperidine (TEMP) as the spin-trapping reagent under solar light irradiation in **Fig. S8**, with an intensity ratio of 1:1:1 that corresponded to the 2,2,6,6-tetramethylpiperidine N-oxyl (TEMPO) adduct. [56, 57], The EPR studies indicated that •O_2^- and $^1O_2$ were the dominant active species that were produced in this catalytic system. h^+ is usually regarded as the other dominant active species of g-C_3N_4. Thereby, free radicals trapping experiments were performed by using KI and BQ as h^+ and •O_2^- scavengers, respectively (**Fig. S9)**. The photocatalytic degradation of RhB over g-C_3N_4/ZnTcPc/0.1GQDs was inhibited apparently after the addition of KI, suggesting that h^+ was another main active species in the photocatalytic process. Likewise, the degrading efficiency of RhB decreased in the presence of 1 mM BQ, which indicated a good agreement between the above EPR results.

The photocurrent-time measurement was deemed as an efficient way to prove the separation efficiency of photogenerated electron-hole pairs. As shown in **Fig. 7a**, g-C_3N_4/ZnTcPc/0.1GQDs exhibited the best photocurrent density response to light irradiation. This further demonstrated that the photogenerated electron-hole pairs of g-C_3N_4/ZnTcPc/0.1GQDs could be separated

efficiently compared with g-C_3N_4 and g-C_3N_4/ZnTcPc though electronic transmission between g-C_3N_4 with ZnTcPc and GQDs.

From the results we have obtained, the possible photocatalytic mechanism for the target substrates degradation by g-C_3N_4/ZnTcPc/0.1GQDs under solar light irradiation is proposed in **Fig. 8**. For ZnTcPc, the CB and VB were more negative than that of g-C_3N_4 [37]. Under solar light irradiation, g-C_3N_4 and ZnTcPc could be stimulated simultaneously. The excited electrons could be transferred from the lowest unoccupied molecular orbital (LUMO) of ZnTcPc to the conduction band of g-C_3N_4, while the photogenerated electrons on the CB of g-C_3N_4 can be further transferred to the GQDs surface rapidly to produce $\bullet O_2^-$, making photogenerated electrons-holes pair separation more effective and reducing the recombination probability. The formed $\bullet O_2^-$ and h^+ played an important role in the degradation of the above pollutants. On the other hand, the generation of $^1O_2$ may be attributed to the transformation between the ground state ZnTcPc and the excited state of ^{1}ZnTcPc and ^{3}ZnTcPc [58]. In summary, $\bullet O_2^-$, h^+, and $^1O_2$ formed during the photocatalytic process lead to effective photocatalytic performance in the g-C_3N_4/ZnTcPc/0.1GQDs catalytic system.

3.3.2 Degradation pathway

Notwithstanding the target substrates can be degraded efficiently by g-C_3N_4/ZnTcPc/GQDs, transformation intermediates generated during the photocatalytic degradation may be underlying environmental pollutants. Consequently, the degradation intermediates of RhB, SQXNa and

CBZ at different reaction times and the final products were analyzed using UPLC/HDMS. The UPLC chromatograms of RhB at different reaction times (0, 20, 30, 40, 50, and 60 min) are displayed in **Fig. 9a**. According to the UPLC chromatograms, peak A(t_R 4.70 min) was the maternal RhB, and peak B (t_R 3.66 min), C (t_R 2.60 min), D (t_R 2.33 min), E (t_R 1.39 min) and F (t_R 0.97 min) were N-de-ethylated intermediates derived from the initial RhB [59, 60]. The N-de-ethylated intermediate structures were detected by HDMS identification and these details are presented in **Table. S1**. As can be seen, the intensity of peak A (RhB) decreased rapidly after reaction for 20min (**Fig. 9a**), while the intensity of N-de-ethylated intermediates (B-E) increased initially and then decreased (**Fig. 9b**). The peak of F increased during the first 60 min and it was degraded after solar light irradiation. All N-de-ethylated intermediates underwent ring-opening mineralization, and eventually produced some biodegradable small molecular acids (**Table S2)**. The UPLC/HDMS results allowed us to propose the possible degradation pathway of RhB (see **Fig. 10**). The N-ethyl group on the maternal RhB molecule was readily attacked by the active radicals [61], making for the formation of N-de-ethylated intermediates. The opening-ring and mineralization process took place subsequently, and benzoic acid, phthalicacid (G, H), and eight biodegradable small molecular acids (P_1-P_8) were produced by the cleavage of RhB and the N-de-ethylated intermediates with the extension of time.

Furthermore, we also propose the probable degradation pathway of SQXNa and CBZ over g-C_3N_4/ZnTcPc/GQDs under solar irradiation according to the UPLC/HDMS results (**Fig.11** and

Fig.S10). The retention time of SQXNa was 4.15 min in the positive mode and the $[SQ\text{-}Na+H]^+$ ion at m/z 301.0757 was yielded. Seven intermediates (F_2–F_8) are monitored in positive and negative ion modes. The corresponding parameters of these intermediates are listed in **Tables S3**. Firstly, the initial photodegradation products of SQXNa may undergo hydroxylation of the quinoxalin moiety to produce intermediates F_2 at m/z = 315.0597 [62], afterwards, intermediate F_5 was produced via the loss of the aniline group. Intermediate F_3 that has the same mass charge ratio as F_2 may be assumed to result from the ammonia molecule that was attacked by •OH, and which lead to the formation of 4-(hydroxyamino)-N-(quinoxalin-2-yl)benzenesulfonamide [63]. Another degradation pathway was that SO_2 can be extruded easily from sulfonamides during the photocatalytic process, resulting in the F_4 ion (m/z = 237.1140) with the molecular formula of $C_{14}H_{12}N_4$ [64, 65]. Subsequently, it was speculated that intermediate F_7 (m/z=180.0815) was oxidized further to the compound at m/z = 253.1089 through •OH attack. The F_6 ion at m/z = 253.1089 could be generated through SO_2 extrusion from the F_3 ion. The intermediate F_8 was formed by further oxidation of intermediate F_5-F_7. Finally, UPLC/HDMS was used to monitor the final products for the determination of SQXNa, but small molecular acids were not detected. We deduced that the mineralization of all intermediates into CO_2 and H_2O would occur, which was consistent with the results of TOC. The major degradation intermediates of CBZ detected by UPLC-Synapt G2-S HDMS were list in **Table S4**. **Figure S10** shows a possible degradation pathway of CBZ. Because the CBZ molecule's 10,11-double bond can be attacked by the reactive species easily [66, 67], C_1 and C_2 were observed at m/z = 253.0977 ($[M+H]^+$) as the

initial photodegradation products. On the other hand, the cleavage of the C10-C11 bond of CBZ can also lead to the formation of intermediate C_4 [68]. Further oxidation of compound C_1 produced the relatively intermediate C_3 and C_5. Compound C_2 (m/z = 253.0977) can be also formed through the ring-contraction reaction of C_1, which could be further oxidized into compound C_8. The intermediates C_6 and C_7 at m/z of 236.0712 and 210.0919 indicate the loss of ammonia (-NH_3) and cyanic acid (-HOCN), respectively. Additionally, the formation of the compound C_9 is attributable to the hydrogen rearrangement reaction with the loss of the -$CONH_2$ group of compound C_2, that may subsequently undergo a second oxidation to yield acridine (compound C_{10} at m/z of 180.0813) [69]. According to the results of TOC, these intermediates can eventually be mineralized into CO_2 and H_2O.

4. Conclusion

In summary, a ternary g-C_3N_4/ZnTcPc/GQDs composite photocatalyst was prepared successfully from g-C_3N_4 co-modified by ZnTcPc and GQDs through chemical bonding and hydrothermal methods. The ternary g-C_3N_4/ZnTcPc/GQDs composite exhibited efficient photocatalytic activity towards RhB, SQXNa and CBZ degradation under solar light irradiation. The introduction of ZnTcPc bonding on the g-C_3N_4 broadened the visible-light response range, and the GQDs dispersed uniformly on g-C_3N_4 surface, which facilitated efficient electrons transfer. Additionally, this system showed excellent photocatalytic performance over a wide pH range,

and the presence of $^1O_2$, $\bullet O_2^-$ and h^+ were the main active species in the photodegradation of pollutants. Based on the UPLC/HDMS results, the photocatalytic degradation pathway for RhB, SQXNa and CBZ was proposed. Consequently, this study provides a novel strategy for the design of a highly efficacious composite photocatalyst to achieve the extension of the visible-light response and the effective charge-separation efficiency simultaneously in environmental remediation.

Author information

Corresponding author

*(W. Lu) E-mail:luwy@zstu.edu.cn; Phone: +86 571 86843611; Fax: +86 571 86843611.

*(W. Chen) E-mail:wxchen@zstu.edu.cn, Phone: +86 571 86843611; Fax: +86 571 86843611.

Author Contributions

The manuscript was written through contributions of all authors. All authors have given approval to the final version of the manuscript.

Notes

The authors declare no competing financial interest.

Acknowledgment

This work was supported by the National Natural Science Foundation of China (No. 51133006 and 51103133), Zhejiang Provincial Natural Science Foundation of China (No. LY14E030013).

Appendix A. Supplementary data

Supplementary data. Supplementary data associated with this article can be found, in the online version, at

References

[1] W.-L. Li, Z.-F. Zhang, W.-L. Ma, L.-Y. Liu, W.-W. Song, Y.-F. Li, Sci. Total Environ. 640-641 (2018) 1139-1147.

[2] A.-K. Ghattas, F. Fischer, A. Wick, T.A. Ternes, Water Res. 116 (2017) 268-295.

[3] E. Archer, B. Petrie, B. Kasprzyk-Hordern, G.M. Wolfaardt, Chemosphere 174 (2017) 437-446.

[4] F. Bonvin, J. Omlin, R. Rutler, W.B. Schweizer, P.J. Alaimo, T.J. Strathmann, K. McNeill, T. Kohn, Environ. Sci. Technol. 47 (2013) 6746-6755.

[5] A. Mirzaei, Z. Chen, F. Haghighat, L. Yerushalmi, Chemosphere 174 (2017) 665-688.

[6] B.N. Bhadra, I. Ahmed, S. Kim, S.H. Jhung, Chem. Eng. J. 314 (2017) 50-58.

[7] C.A. D'Amato, R. Giovannetti, M. Zannotti, E. Rommozzi, S. Ferraro, C. Seghetti, M. Minicucci, R. Gunnella, A. Di Cicco, Appl. Surf. Sci. 441 (2018) 575-587.

[8] A. Mallick, S. Roy, Nanoscale 10 (2018) 12713-12722.

[9] F. Guo, W. Shi, H. Wang, M. Han, W. Guan, H. Huang, Y. Liu, Z. Kang, J. Hazard. Mater. 349 (2018) 111-118.

[10] W.J. Ong, L.L. Tan, Y.H. Ng, S.T. Yong, S.P. Chai, Chem. Rev. 116 (2016) 7159-7329.

[11] X. Wang, K. Maeda, A. Thomas, K. Takanabe, G. Xin, J.M. Carlsson, K. Domen, M. Antonietti, Nat. Mater. 8 (2009) 76-80.

[12] S. Yang, Y. Gong, J. Zhang, L. Zhan, L. Ma, Z. Fang, R. Vajtai, X. Wang, P.M. Ajayan, Adv. Mater. 25 (2013) 2452-2456.

[13] M. Zhu, S. Kim, L. Mao, M. Fujitsuka, J. Zhang, X. Wang, T. Majima, J. Am. Chem. Soc. 139 (2017) 13234-13242.

[14] Y. He, L. Zhang, B. Teng, M. Fan, Environ. Sci. Technol. 49 (2015) 649-656.

[15] W.J. Ong, L.L. Tan, S.P. Chai, S.T. Yong, Chem. Commun. 51 (2015) 858-861.

[16] H. Shi, G. Chen, C. Zhang, Z. Zou, ACS Catal. 4 (2014) 3637-3643.

[17] Y. Gong, X. Zhao, H. Zhang, B. Yang, K. Xiao, T. Guo, J. Zhang, H. Shao, Y. Wang, G. Yu, Appl. Catal. B Environ. 233 (2018) 35-45.

[18] F. Chen, Q. Yang, Y. Wang, F. Yao, Y. Ma, X. Huang, X. Li, D. Wang, G. Zeng, H. Yu, Chem. Eng. J. 348 (2018) 157-170.

[19] X. Wang, F. Wang, C. Bo, K. Cheng, J. Wang, J. Zhang, H. Song, Appl. Surf. Sci. 453 (2018) 320-329.

[20] Y. Wang, W. Yang, X. Chen, J. Wang, Y. Zhu, Appl. Catal. B Environ. 220 (2018) 337-347.

[21] H. Shao, X. Zhao, Y. Wang, R. Mao, Y. Wang, M. Qiao, S. Zhao, Y. Zhu, Appl. Catal. B Environ. 218 (2017) 810-818.

[22] M.A. Mohamed, M.F. M. Zain, L. Jeffery Minggu, M.B. Kassim, N.A. Saidina Amin, W.N. W. Salleh, M.N.I. Salehmin, M.F. Md Nasir, Z.A. Mohd Hir, Appl. Catal. B Environ. 236 (2018) 265-279.

[23] M. Jourshabani, Z. Shariatinia, A. Badiei, Appl. Surf. Sci. 427 (2018) 375-387.

[24] O. Fontelles-Carceller, M.J. Munoz-Batista, M. Fernandez-Garcia, A. Kubacka, ACS Appl. Mater. Interfaces 8 (2016) 2617-2627.

[25] C.H. Choi, L. Lin, S. Gim, S. Lee, H. Kim, X. Wang, W. Choi, ACS Catal. 8 (2018) 4241-4256.

[26] X.-H. Li, J. Zhang, X. Chen, A. Fischer, A. Thomas, M. Antonietti, X. Wang, Chem. Mater. 23 (2011) 4344-4348.

[27] Q. Han, B. Wang, Y. Zhao, C. Hu, L. Qu, Angew. Chem. Int. Ed. 54 (2015) 11433-11437.

[28] J. Xu, Z. Wang, Y. Zhu, ACS Appl. Mater. Interfaces 9 (2017) 27727-27735.

[29] Y. Chen, X. Wang, J. Phys. Chem. C 122 (2018) 3786-3793.

[30] J. Wang, Y. Zheng, T. Peng, J. Zhang, R. Li, ACS Sustainable Chem. Eng. 5 (2017) 7549-7556.

[31] J. Qin, J. Huo, P. Zhang, J. Zeng, T. Wang, H. Zeng, Nanoscale 8 (2016) 2249-2259.

[32] J. Xu, Y. Li, S. Peng, G. Lu, S. Li, Phys. Chem. Chem. Phys. 15 (2013) 7657-7665.

[33] H. Imahori, T. Umeyama, S. Ito, Accounts Chem. Res. 42 (2009) 1809-1818.

[34] P. Brogdon, H. Cheema, J.H. Delcamp, ChemSusChem 11 (2018) 86-103.

[35] D.O. Oluwole, F.A. Sarı, E. Prinsloo, E. Dube, A. Yuzer, T. Nyokong, M. Ince, Spectrochim. Acta A 203 (2018) 236-243.

[36] A.B. Sorokin, Chem. Rev. 113 (2013) 8152-8191.

[37] W. Lu, T. Xu, Y. Wang, H. Hu, N. Li, X. Jiang, W. Chen, Appl. Catal. B Environ. 180 (2016) 20-28.

[38] L. Ge, C. Han, Appl. Catal. B Environ. 117-118 (2012) 268-274.

[39] K.C. Christoforidis, Z. Syrgiannis, V. La Parola, T. Montini, C. Petit, E. Stathatos, R. Godin, J.R. Durrant, M. Prato, P. Fornasiero, Nano Energy 50 (2018) 468-478.

[40] J. Liu, Y. Liu, N. Liu, Y. Han, X. Zhang, H. Huang, Y. Lifshitz, S.-T. Lee, J. Zhong, Z. Kang, Science 347 (2015) 970.

[41] W.-J. Ong, L.K. Putri, Y.-C. Tan, L.-L. Tan, N. Li, Y.H. Ng, X. Wen, S.-P. Chai, Nano Res. 10 (2017) 1673-1696.

[42] X. Miao, X. Shen, J. Wu, Z. Ji, J. Wang, L. Kong, M. Liu, C. Song, Appl. Catal. A Gen. 539 (2017) 104-113.

[43] J. Liu, H. Xu, Y. Xu, Y. Song, J. Lian, Y. Zhao, L. Wang, L. Huang, H. Ji, H. Li, Appl. Catal. B Environ. 207 (2017) 429-437.

[44] M. Yan, Y. Hua, F. Zhu, L. Sun, W. Gu, W. Shi, Appl. Catal. B Environ. 206 (2017) 531-537.

[45] J. Liu, T. Zhang, Z. Wang, G. Dawson, W. Chen, J. Mater. Chem. 21 (2011) 14398.

[46] F. Dong, L. Wu, Y. Sun, M. Fu, Z. Wu, S.C. Lee, J. Mater. Chem. 21 (2011) 15171.

[47] J. Chen, N. Chen, J. Huang, J. Wang, M. Huang, Inorg. Chem. Commun. 9 (2006) 313-315.

[48] T.F. Yeh, C.Y. Teng, S.J. Chen, H. Teng, Adv. Mater. 26 (2014) 3297-3303.

[49] J. Hu, H. Liu, L. Wang, N. Li, T. Xu, W. Lu, Z. Zhu, W. Chen, Carbon 100 (2016) 408-416.

[50] J. Zhang, S. Sun, Y. Bian, W. Li, R. Liu, D. Zhao, Fuel 220 (2018) 513-520.

[51] H. Yan, H. Yang, J. Alloys Compd. 509 (2011) L26-L29.

[52] H. Ji, F. Chang, X. Hu, W. Qin, J. Shen, Chem. Eng. J. 218 (2013) 183-190.

[53] J. Song, X. Wang, J. Ma, X. Wang, J. Wang, S. Xia, J. Zhao, Chem. Eng. J. 348 (2018) 380-388.

[54] F. Wu, H. Huang, T. Xu, W. Lu, N. Li, W. Chen, Appl. Catal. B Environ. 218 (2017) 230-239.

[55] H. Wang, D. Yong, S. Chen, S. Jiang, X. Zhang, W. Shao, Q. Zhang, W. Yan, B. Pan, Y. Xie, J. Am. Chem. Soc. 140 (2018) 1760-1766.

[56] S. Xu, P. Zhou, Z. Zhang, C. Yang, B. Zhang, K. Deng, S. Bottle, H. Zhu, J. Am. Chem. Soc. 139 (2017) 14775-14782.

[57] H. Wang, S. Jiang, S. Chen, D. Li, X. Zhang, W. Shao, X. Sun, J. Xie, Z. Zhao, Q. Zhang, Y. Tian, Y. Xie, Adv. Mater. 28 (2016) 6940-6945.

[58] M. Gao, N. Li, W. Lu, W. Chen, Appl. Catal. B Environ. 147 (2014) 805-812.

[59] X. Li, T. Wan, J. Qiu, H. Wei, F. Qin, Y. Wang, Y. Liao, Z. Huang, X. Tan, Appl. Catal. B Environ. 217 (2017) 591-602.

[60] B. Li, C. Lai, G. Zeng, L. Qin, H. Yi, D. Huang, C. Zhou, X. Liu, M. Cheng, P. Xu, C. Zhang, F. Huang, S. Liu, ACS Appl. Mater. Interfaces 10 (2018) 18824-18836.

[61] T. Xu, D. Ni, X. Chen, F. Wu, P. Ge, W. Lu, H. Hu, Z. Zhu, W. Chen, J. Hazard. Mater. 317 (2016) 17-26.

[62] Z. Zhu, W. Lu, N. Li, T. Xu, W. Chen, Chem. Eng. J. 321 (2017) 58-66.

[63] Q.-N. Liao, F. Ji, J.-C. Li, X. Zhan, Z.-H. Hu, Chem. Eng. J. 284 (2016) 494-502.

[64] A.L. Boreen, W.A. Arnold, K. McNeill, Environ. Sci. Technol. 39 (2005) 3630-3638.

[65] D. Qin, W. Lu, X. Wang, N. Li, X. Chen, Z. Zhu, W. Chen, ACS Appl. Mater. Interfaces 8 (2016) 25962-25970.

[66] Y. Pan, S. Cheng, X. Yang, J. Ren, J. Fang, C. Shang, W. Song, L. Lian, X. Zhang, Water Res. 116 (2017) 254-265.

[67] B. Yang, R.S. Kookana, M. Williams, J. Du, H. Doan, A. Kumar, Water Res. 100 (2016) 413-420.

[68] J. Xu, L. Li, C. Guo, Y. Zhang, W. Meng, Appl. Catal. B Environ. 130-131 (2013) 285-292.

[69] C. Martínez, M. Canle L, M.I. Fernández, J.A. Santaballa, J. Faria, Appl. Catal. B Environ. 102 (2011) 563-571.

Figure Captions

Fig. 1. TEM images of g-C_3N_4 (a,b,c), g-C_3N_4/ZnTcPc (d,e,f) and, g-C_3N_4/ZnTcPc/0.1GQDs (g,h,i).

Fig. 2. UV-vis DRS absorption spectrum of g-C_3N_4, g-C_3N_4/ZnTcPc and g-C_3N_4/ZnTcPc/0.1GQDs.

Fig. 3. FTIR (a) and XRD (b) spectra of ZnTcPc, g-C_3N_4, g-C_3N_4/ZnTcPc, g-C_3N_4/ZnTcPc/0.1GQDs.

Fig. 4. Curve fit of the C 1s peak of (a) g-C_3N_4, (b) g-C_3N_4/ZnTcPc and (c) g-C_3N_4/ZnTcPc/0.1GQDs.

Fig. 5. (a) Photocatalytic degradation of RhB in the presence of g-C_3N_4, g-C_3N_4/ZnTcPc and g-C_3N_4/ZnTcPc/0.1GQDs under solar light irradiation, pH=5.3; (b) Photocatalytic degradation of CBZ and SQXNa in the presence of g-C_3N_4/ZnTcPc/0.1GQDs under solar light irradiation, (c) The removal rate of RhB at different pH in the presence of g-C_3N_4/ZnTcPc/0.1GQDs under soalr light irradiation. (d) The cyclic catalytic oxidation of RhB under solar light irradiation after 60 min. [RhB] =20 μM， [CBZ] = [SQXNa] = 25 μM, [g-C_3N_4]=[ZnTcPc]=[g-C_3N_4/ZnTcPc]= [g-C_3N_4/ZnTcPc+0.1GQDs]= [g-C_3N_4/ZnTcPc/0.1GQDs]=0.1 g/L.

Fig. 6. DMPO spin-trapping EPR spectra in aqueous or methanol solutions in the presence of g-C_3N_4, g-C_3N_4/ZnTcPc and g-C_3N_4/ZnTcPc/0.1GQDs under solar light irradiation, (a) aqueous solution; (b) methanol solution. [DMPO]=10 mM.

Fig. 7. (a) Transient photocurrent density response of g-C_3N_4, g-C_3N_4/ZnTcPc and g-C_3N_4/ZnTcPc/0.1GQDs photocatalysts electrodes with light on-off cycles under solar light irradiation, [Na_2SO_4] = 0.1 M; (b) Photoluminescence (PL) spectra of g-C_3N_4, g-C_3N_4/ZnTcPc and g-C_3N_4/ZnTcPc/0.1GQDs.

Fig. 8. Schematic diagram of possible reaction mechanism over g-C_3N_4/ZnTcPc/0.1GQDs photocatalyst under solar light irradiation.

Fig. 9. Temporal UPLC spectra profiles (a) and temporal change in the distribution of the N-de-ethylated intermediates (b) during the photocatalytic degradation of RhB from UPLC Sy

Fig. 10. Possible pathway for the photocatalytic degradation of RhB over g-C_3N_4/ZnTcPc/0.1GQDs photocatalyst under solar light irradiation. [RhB] = 20 μM.

Fig. 11. Possible pathway for the photocatalytic degradation of SQXNa over g-C_3N_4/ZnTcPc/0.1GQDs photocatalyst under solar light irradiation. [SQXNa] = 25 μM.

Scheme 1. Schematic for the synthesis process of g-C_3N_4/ZnTcPc/GQDs.

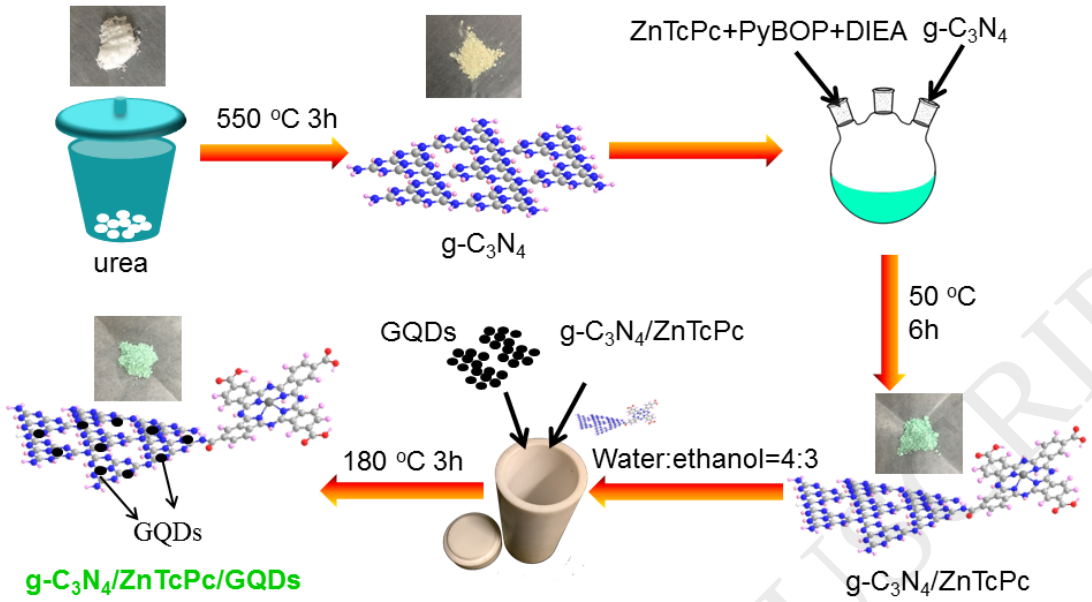

Scheme 1. Schematic for the synthesis process of g-C_3N_4/ZnTcPc/GQDs.

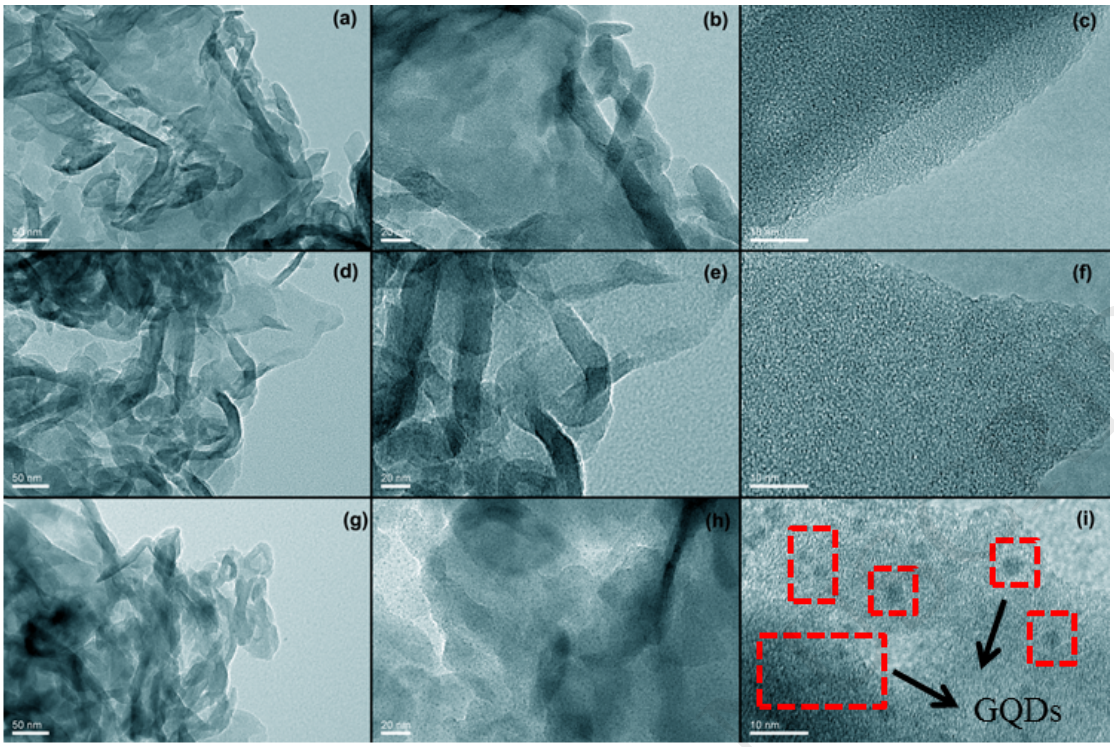

Fig. 1. TEM images of g-C_3N_4 (a,b,c), g-C_3N_4/ZnTcPc (d,e,f) and, g-C_3N_4/ZnTcPc/0.1GQDs (g,h,i).

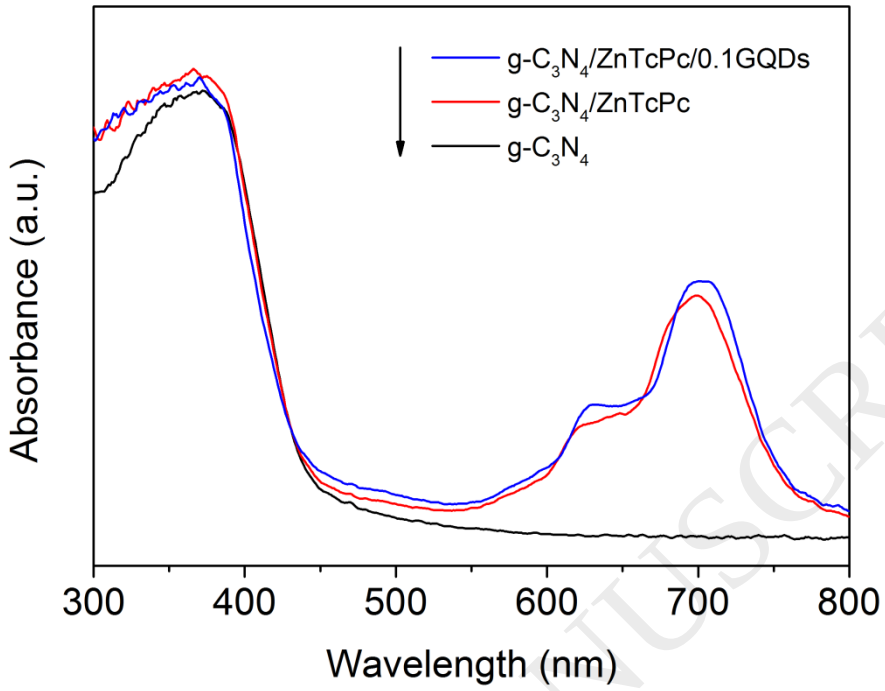

Fig. 2. UV-vis DRS absorption spectrum of g-C_3N_4, g-C_3N_4/ZnTcPc and g-C_3N_4/ZnTcPc/0.1GQDs.

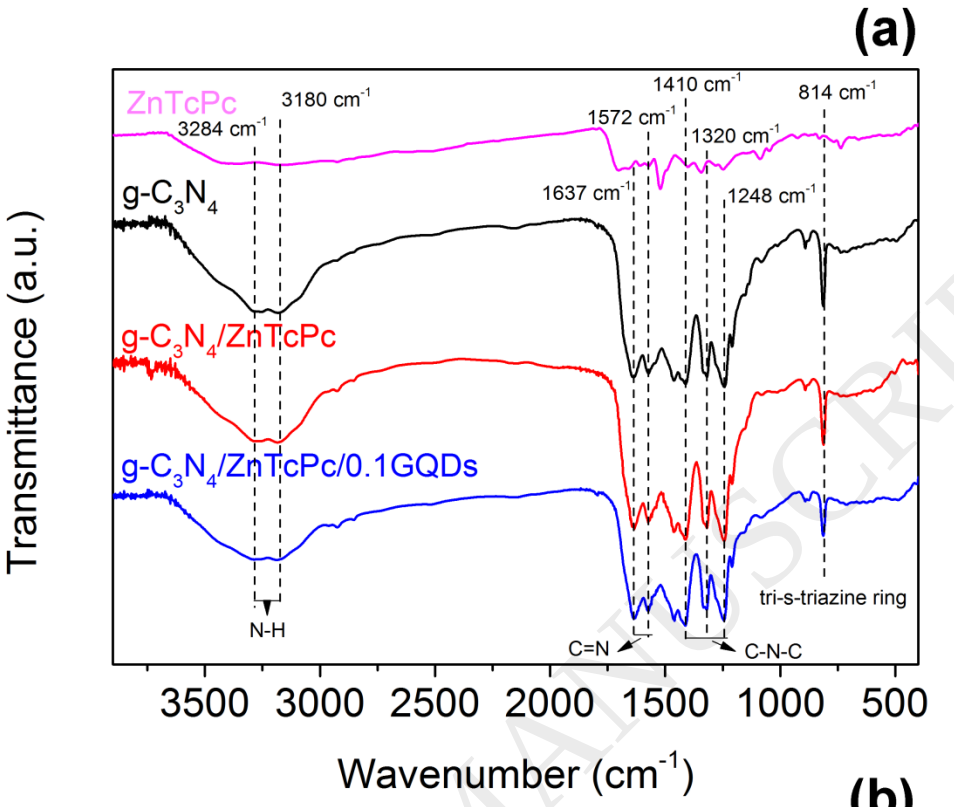

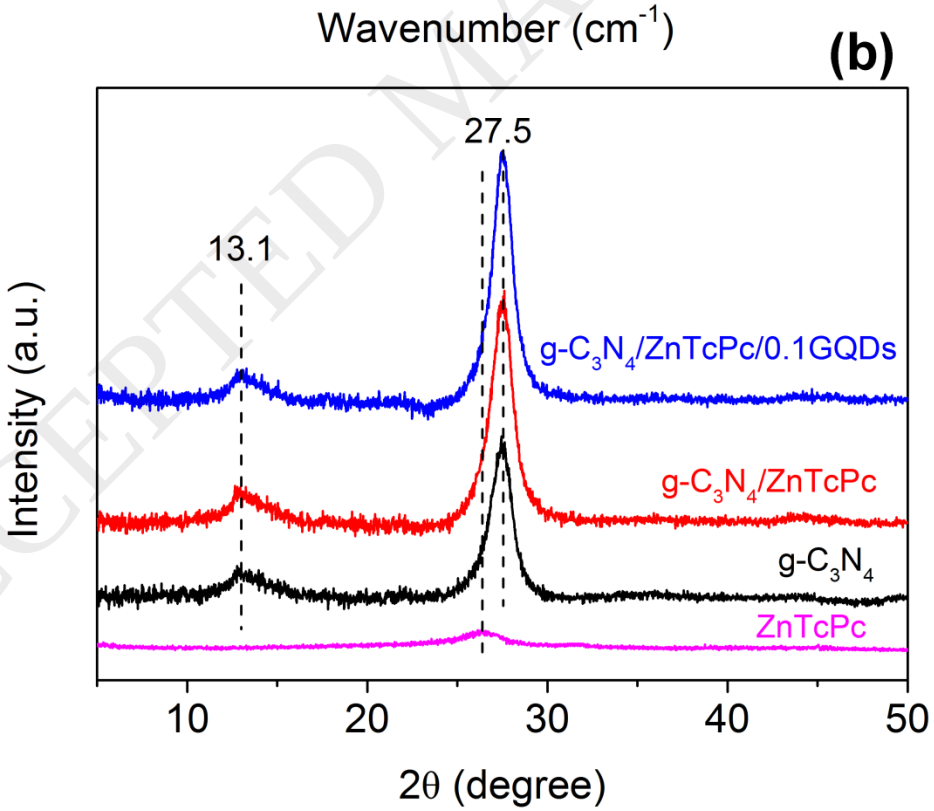

Fig. 3. FTIR (a) and XRD (b) spectra of ZnTcPc, g-C_3N_4, g-C_3N_4/ZnTcPc, g-C_3N_4/ZnTcPc/0.1GQDs.

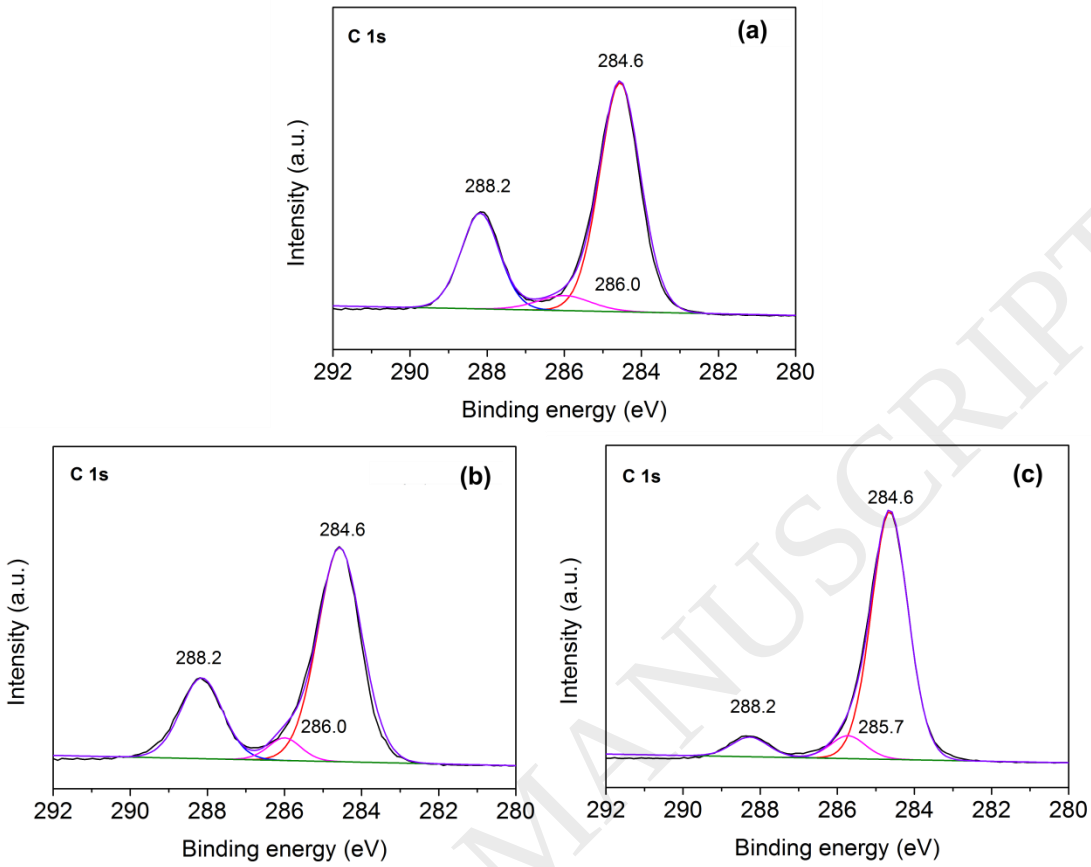

Fig. 4. Curve fit of the C 1s peak of (a) g-C_3N_4, (b) g-C_3N_4/ZnTcPc and (c) g-C_3N_4/ZnTcPc/0.1GQDs.

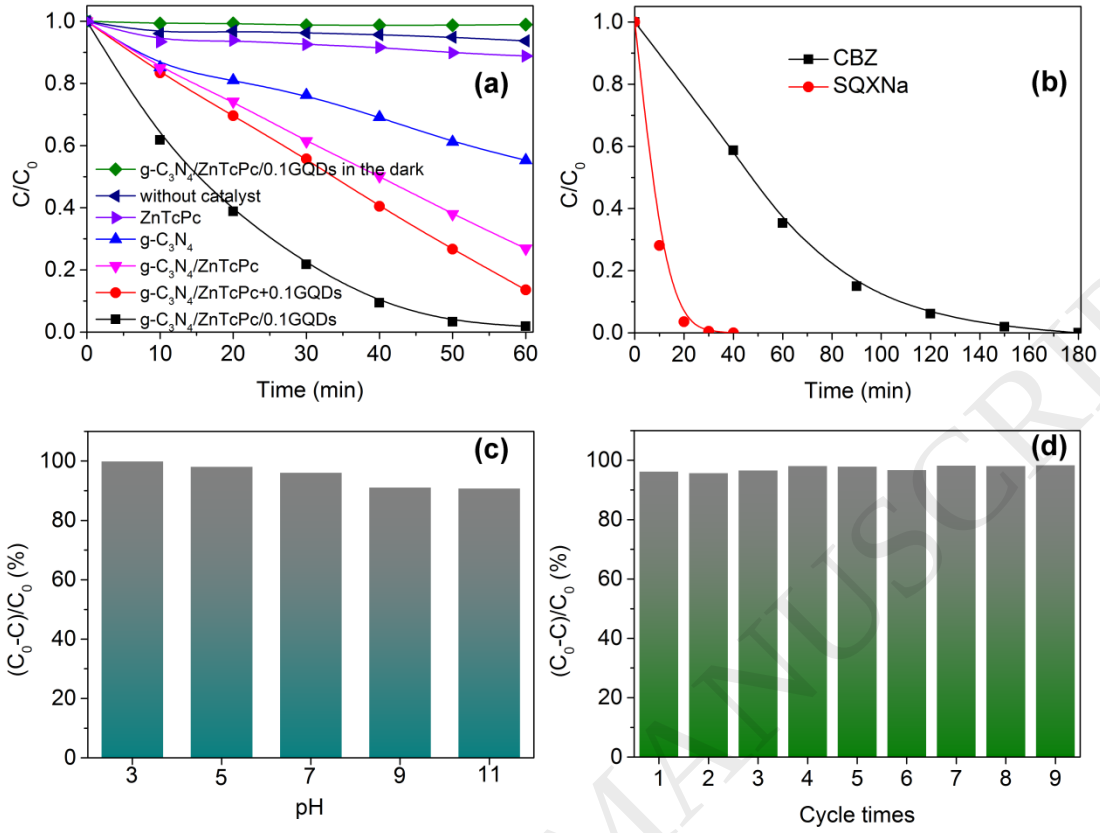

Fig. 5. (a) Photocatalytic degradation of RhB in the presence of g-C_3N_4, g-C_3N_4/ZnTcPc and g-C_3N_4/ZnTcPc/0.1GQDs under solar light irradiation, pH=5.3; (b) Photocatalytic degradation of CBZ and SQXNa in the presence of g-C_3N_4/ZnTcPc/0.1GQDs under solar light irradiation, (c) The removal rate of RhB at different pH in the presence of g-C_3N_4/ZnTcPc/0.1GQDs under soalr light irradiation. (d) The cyclic catalytic oxidation of RhB under solar light irradiation after 60 min. [RhB] =20 μM， [CBZ] = [SQXNa] = 25 μM, [g-C_3N_4]=[ZnTcPc]=[g-C_3N_4/ZnTcPc]= [g-C_3N_4/ZnTcPc+0.1GQDs]= [g-C_3N_4/ZnTcPc/0.1GQDs]=0.1 g/L.

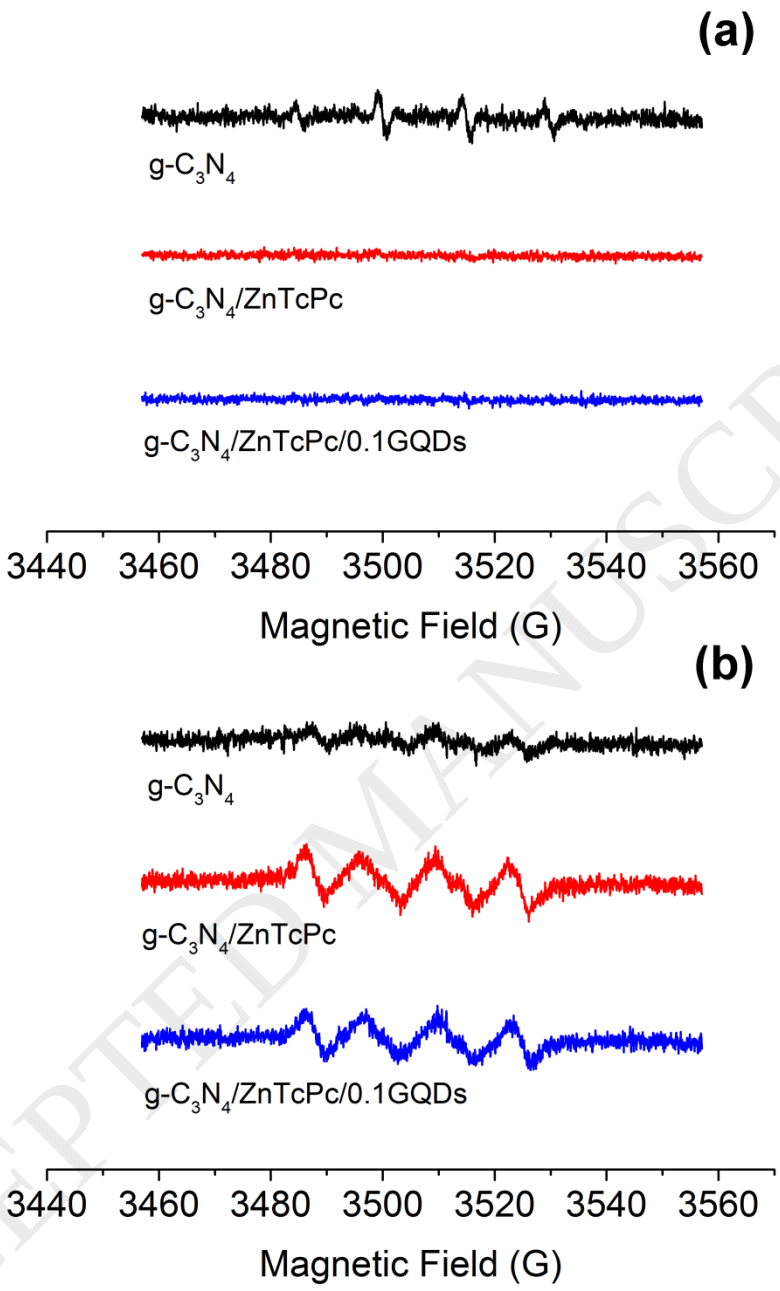

Fig. 6. DMPO spin-trapping EPR spectra in aqueous or methanol solutions in the presence of g-C_3N_4, g-C_3N_4/ZnTcPc and g-C_3N_4/ZnTcPc/0.1GQDs under solar light irradiation, (a) aqueous solution; (b) methanol solution. [DMPO]=10 mM.

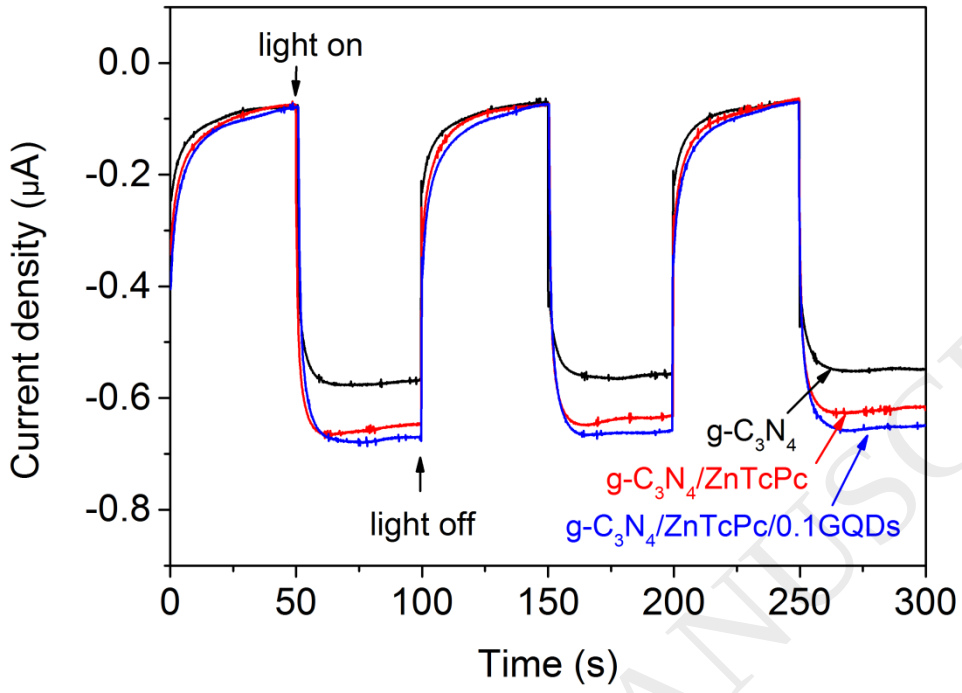

Fig. 7. (a) Transient photocurrent density response of g-C_3N_4, g-C_3N_4/ZnTcPc and g-C_3N_4/ZnTcPc/0.1GQDs photocatalysts electrodes with light on-off cycles under solar light irradiation, [Na_2SO_4] = 0.1 M; (b) Photoluminescence (PL) spectra of g-C_3N_4, g-C_3N_4/ZnTcPc and g-C_3N_4/ZnTcPc/0.1GQDs.

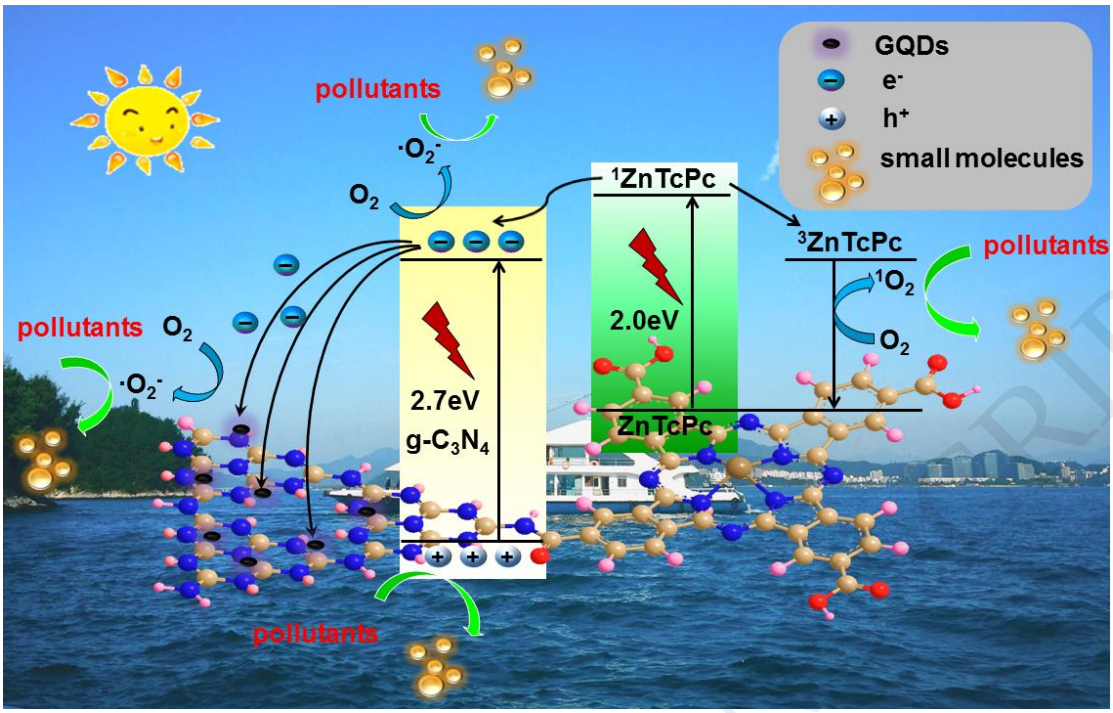

Fig. 8. Schematic diagram of possible reaction mechanism over g-C_3N_4/ZnTcPc/0.1GQDs photocatalyst under solar light irradiation.

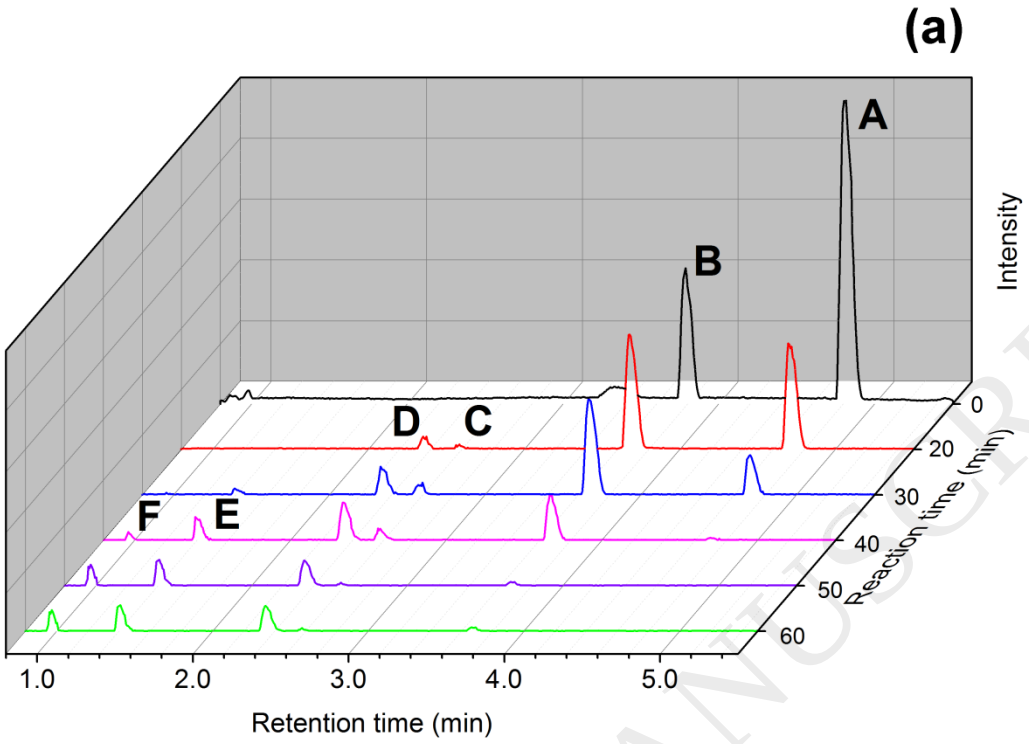

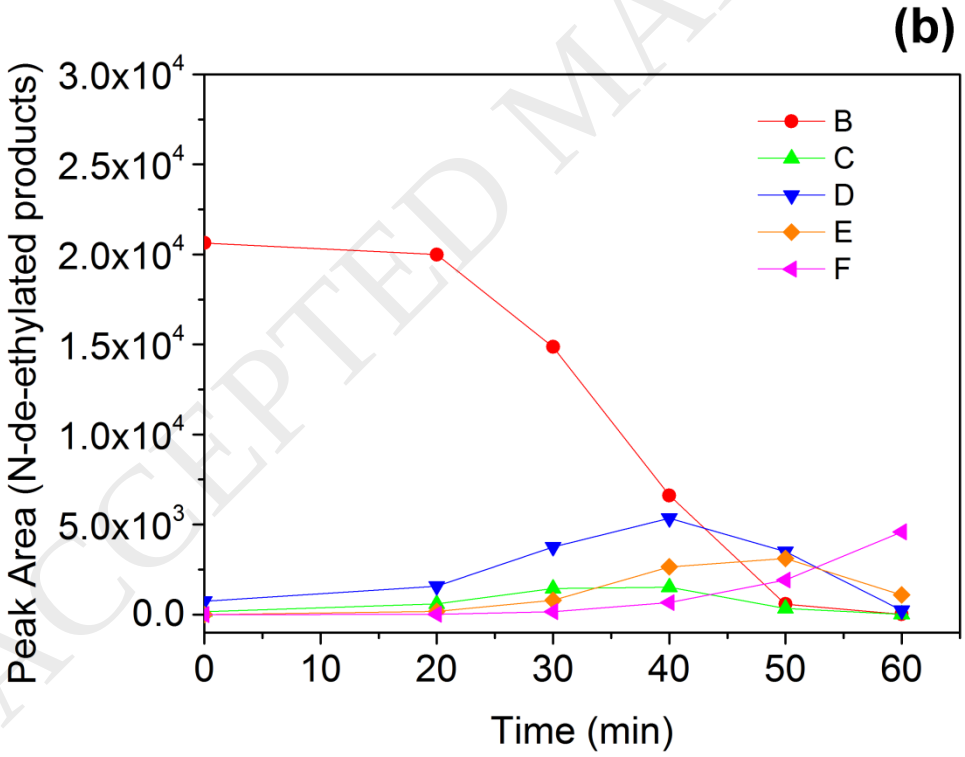

Fig. 9. Temporal UPLC spectra profiles (a) and temporal change in the distribution of the N-de-ethylated intermediates (b) during the photocatalytic degradation of RhB from UPLC Synapt G2-S HDMS. [RhB] = 20 µM.

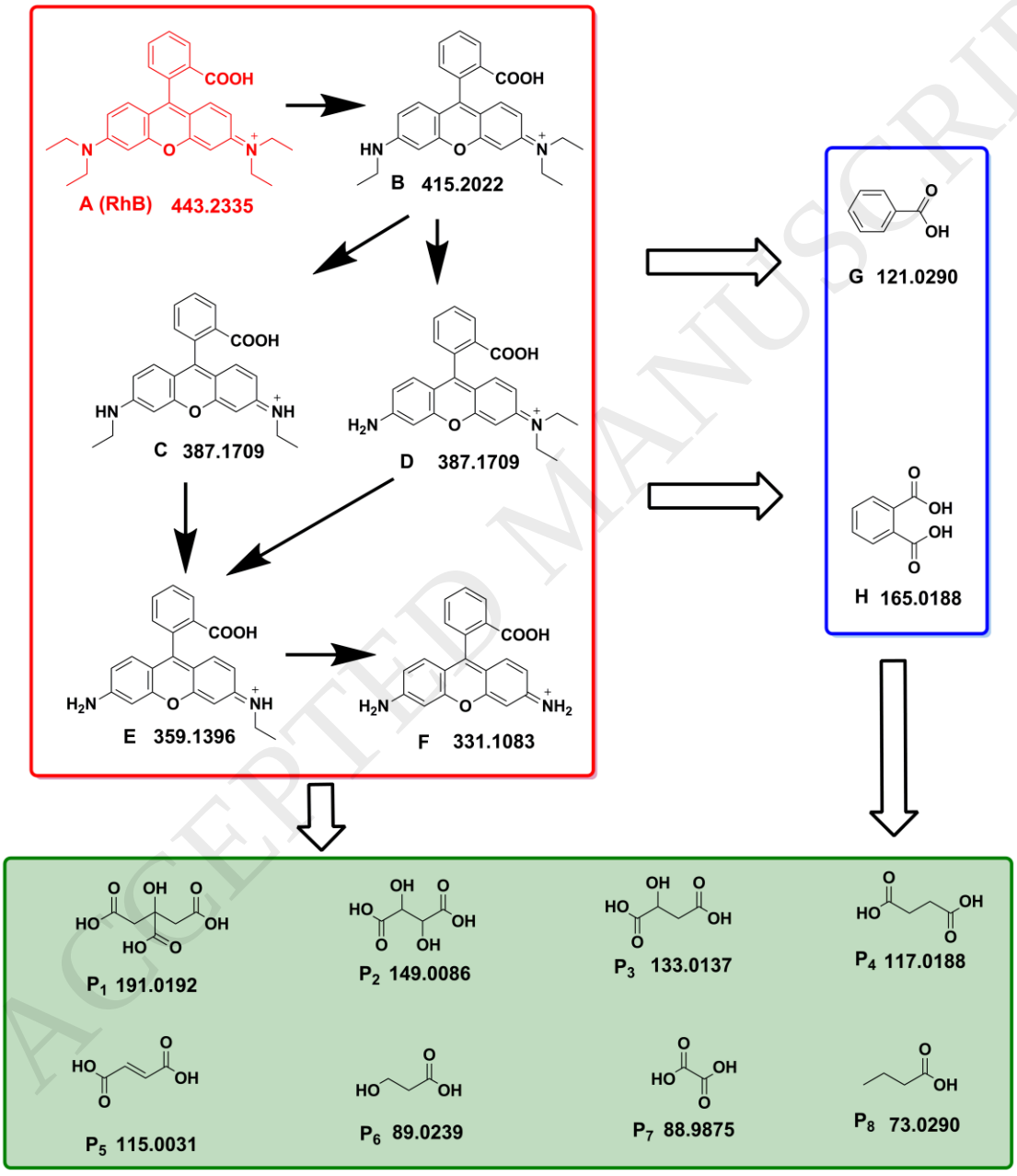

Fig. 10. Possible pathway for the photocatalytic degradation of RhB over g-C_3N_4/ZnTcPc/0.1GQDs photocatalyst under solar light irradiation. [RhB] = 20 µM.

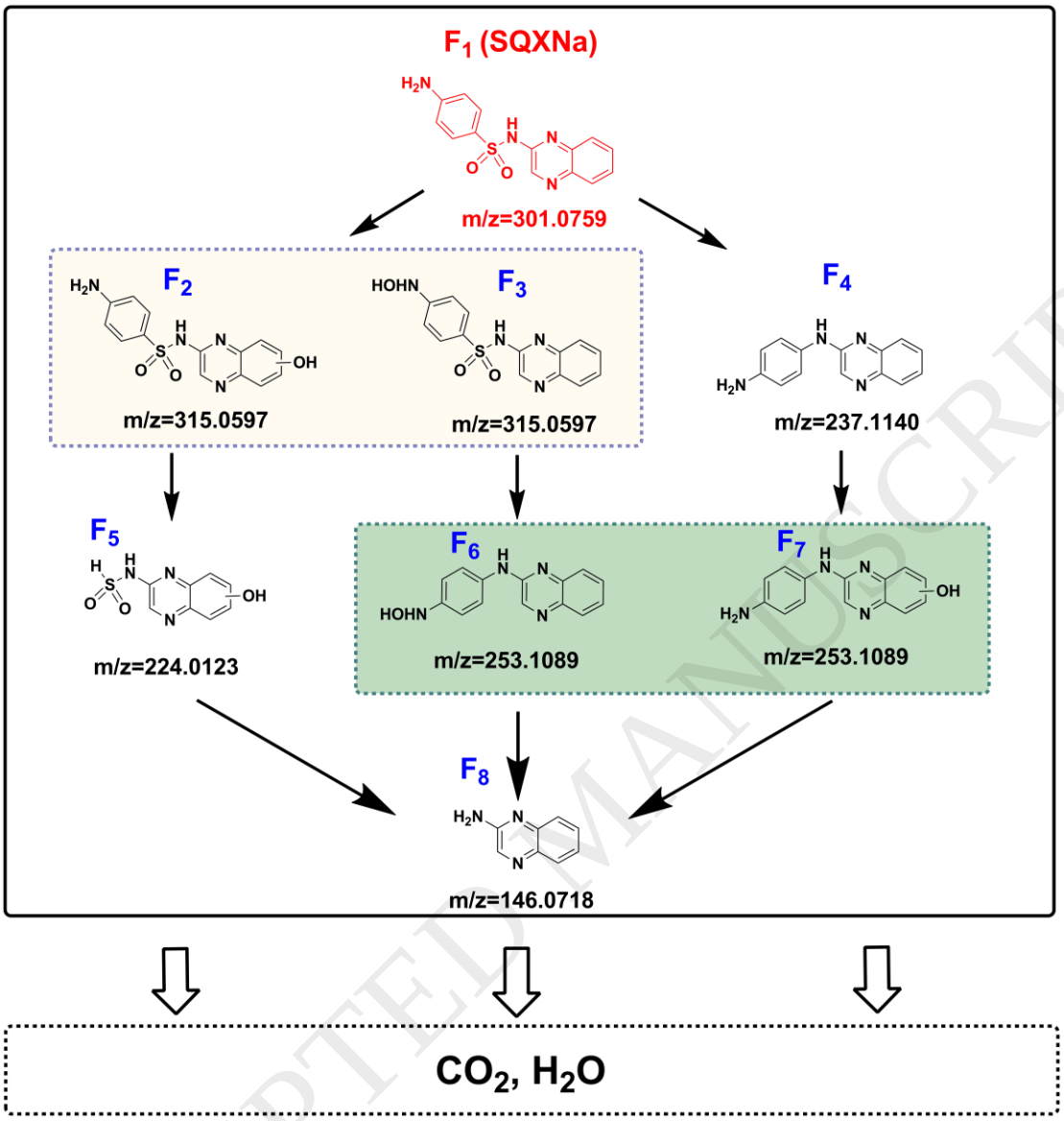

Fig. 11. Possible pathway for the photocatalytic degradation of SQXNa over g-C_3N_4/ZnTcPc/0.1GQDs photocatalyst under solar light irradiation. [SQXNa] = 25 µM.